Segmentation of optic disc in retinal images for glaucoma diagnosis by saliency level set with enhanced active contour model

Sobia Naz, Kabbinale Ananda Radhakrishna Rao

Department of Electronics and Communication Engineering, P.E.S. College of Engineering, Karnataka, India

Article Info

ABSTRACT

Glaucoma is an ophthalmic disease which is among the chief causes of visual impairment across the globe. The clarity of the optic disc (OD) is crucial for recognizing glaucoma. Since existing methods are unable to successfully integrate multi-view information derived from shape and appearance to precisely explain OD for segmentation, this paper proposes a saliency-based level set with an enhanced active contour method (SL-EACM), a modified locally statistical active contour model, and entropy-based optical disc localization. The significant contributions are that i) the SL-EACM is introduced to address the often noticed problem of intensity inhomogeneity brought on by defects in imaging equipment or fluctuations in lighting; ii) to prevent the integrity of the OD structures from being compromised by pathological alterations and artery blockage, local image probability data is included from a multi-dimensional feature space around the region of interest in the model; and iii) the model incorporates prior shape information into the technique, for enhancing the accuracy in identifying the OD structures from surrounding regions. Public databases such as CHASE_DB, DRIONS-DB, and Drishti-GS are used to evaluate the proposed model. The findings from numerous trials demonstrate that the proposed model outperforms state-of-the-art approaches in terms of qualitative and quantitative outcomes.

This is an open access article under the CC BY-SA license.

Corresponding Author:

Sobia Naz
Department of Electronics and Communication Engineering, P.E.S. College of Engineering
Mandya, Karnataka-571401, India
Email: sobia.pesce@gmail.com

1. INTRODUCTION

Glaucoma is a condition that causes blindness in an individual. This eye disease is the third leading cause of blindness in India [1]. Due to a restriction in intraocular fluid outflow, glaucoma is characterized by an increase in intraocular pressure (IOP) in the eye. Glaucoma is often diagnosed by using ophthalmoscopy to study the shape and color of the optic nerve during a manual evaluation of the optic disc (OD). Due to the multiple problems connected with the procedure, detecting anomalies in the human eye, in particular, is tough. Researchers have been paying more attention to retinal image processing as a result of the demand for sickness detection systems [2]. Early detection of glaucoma is crucial for halting the progression of vision impairment. Glaucoma increases the optic cup-to-disc ratio (CDR) which causes peripheral vision loss [3]. The study work [4] investigates different image processing approaches for OD segmentation based on glaucoma assessment of pre-processed fundus images. The outcomes are presented, and the techniques are evaluated using publicly available fundus images. Modern algorithms for glaucoma detection are necessary to prevent human intrusion [5]. The OD's main structures are shown in Figure 1. The region between the

white line and the black line, which represent the boundaries of the OD and the optic cup, respectively, is known as the neuroretinal rim. The peripapillary atrophy (PPA) and the intensity inhomogeneity are depicted in Figure 2. In the great majority of cases, the manual examination of the retinal image results in misdetection due to human error, which is usually caused by visual fatigue [6]. The accuracy of the retinal image screening investigation is improved with the design of a computer-aided diagnosis system (CAD). Certain vascular retinal properties, such as branching pattern, breadth, and length, have led to innovative approaches for detecting infections [7], [8]. The absence of magnification produces distortions that can be used to defend against CDR limitations in accuracy [9]. The CDR value is found to be inconsistent, which helps to explain the degree of OD damage induced by glaucoma. This research primarily aims to create an optimization strategy that will improve the precision of glaucoma detection. This is why an automated CAD system must have OD segmentation and OD center localization [10].
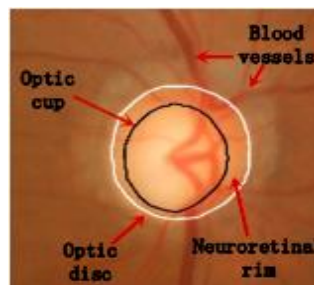

Figure 1. Components of the optical disc

For the purpose of segmenting the OD, several methods have been created to date. They may be loosely divided into two groups: model-based techniques and nonmodel-based approaches. For nonmodel-based algorithms [11], [12] the contours of the OD are recovered using morphological techniques, pixels, clustering, and thresholding. However, intensity inhomogeneity-which impairs the contour extraction OD-often occurs in retinal fundus images, due to image faults in devices or variations in lighting. Shape-based template matching [13]–[16], deformable model approaches [17], [18], and model-based deep learning approaches [19]–[21] are examples of model-based techniques. Considering that the object is round or roughly elliptical, the OD's form can be inferred to be either a circle [13]–[15] or an ellipse [16]. The template-matching techniques based on shape, however, cannot adapt to changes, such as shape irregularity in some areas of the OD caused by various pathological changes or alterations. Many deformable model techniques, which may be further separated into edge-based active contour models [17], [18] and region-based active contour models [22]–[25], have been proposed to address it. Active contour models with edges may fill in the gaps in the image feature being located. Additionally, as they lack a global template structure, they are able to arbitrarily alter the structure of the object. Active contour models based on regions are better able to manage local variations in the OD, but they have trouble with images with varying intensities. However, the disadvantage of active contour model-based approaches is that they ignore the prior information of OD's spatial correlation.

Deep learning has recently gained popularity in the fields of computer vision and pattern recognition and has demonstrated impressive performance. Few deep network-based approaches for the OD's segmentation have been developed [26]–[28]. These methods have certain shortcomings even though they can segment the OD with high performance [29], [30]. The deep network model needs a significant amount of training data with pixel-level annotations in order to be trained for testing, and in the absence of sufficient labelled training samples, the network struggles to achieve promising segmentation results. These networks, however, fail to account for an object's prior knowledge, which leads to the loss of spatial information through max pooling in the encoder and irregular segmentation. By combining the benefits of both types of techniques, this research offers a solution to all the issues stated above and presents two unique energy optimization frameworks. The major contributions include the following: i) the saliency-based level set with an enhanced active contour method (SL-EACM) was created to deal with the harsh inhomogeneity of intensity that is widely present within fundus retinal images; ii) the work adds probability data from a multi-dimensional feature space into the algorithms in order to completely analyze the underlying structure inside fundus retinal pictures and to extract greater integrity from OD borders; and iii) it is better to incorporate the preceding shape constraint data into segmentation approaches when considering the anatomical framework of OD and the ellipse.

The research project is structured: section 2 discusses the evaluation of the current techniques in the literature. Section 3 contains the part on proposed techniques, whereas section 4 displays the results and discussions. Section 5 discusses the study's results and further steps.

Figure 1 displays the components of OD appearance in the fundus image. Figure 2(a) shows the complicated OD appearance is influenced by intensity inhomogeneities, blood vessel occlusions, ill-defined boundaries, irregular form, and certain anomalies such as peripapillary atrophy (PPA). Figure 2(b) shows the variation of color intensity in the OD segmentation.
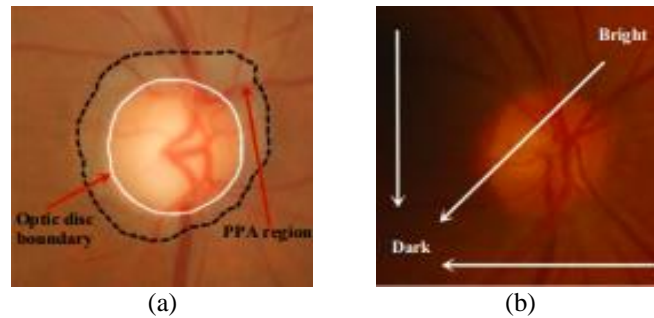

Figure 2. OD intensity (a) inhomogeneity in fundus image and (b) intensity variation in fundus image

2. METHOD

In this research, an effective OD segmentation is performed by using the SL-EACM with entropy-based OD localization. The important process of the proposed method is database acquisition, pre-processing stage, OD localization using entropy, and OD segmentation using SL-EACM. Figure 3 displays a block diagram illustrating the proposed research. The developed SL-EACM method is used to overcome the issues of uneven illumination and enhance the segmentation of OD. The proposed work is evaluated on the Drishti-GS, CHASE_DB1, and DRIONS-DB datasets, which are being discussed in the upcoming section 2.1.
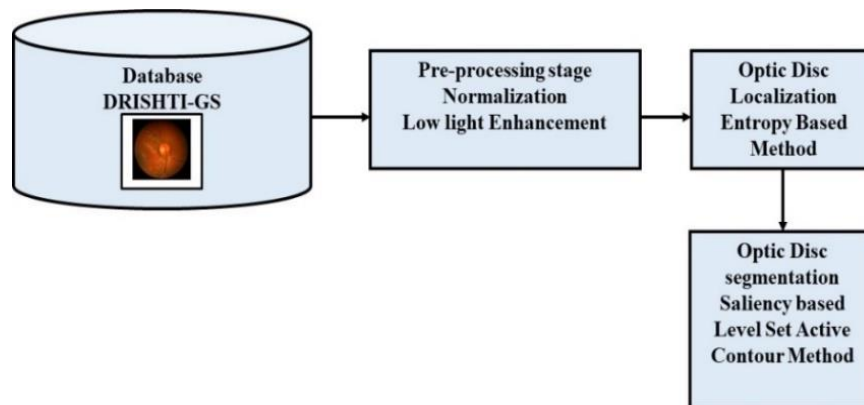

Figure 3. Block diagram depicting the proposed method

2.1. Dataset description
2.1.1. Drishti-GS

Drishti-GS [31] is a dataset for testing OD segmentation, cup detection, and notching detection. Aravind Eye Hospital in Madurai, India, gathered and tagged the images that make up the Drishti-GS collection. A training set and a testing set of photos are included in the dataset. Ground facts for OD and cup segmentation as well as notching information are included in the training photos (50).

2.1.2. CHASE_DB1

Child Health and Study England's CHASE_DB1 [32] is a reference database collected as a part of a health study done across 200 primary schools in London. The CHASE_DB1 database's 28 photos are separated into two groups: a training set (8 Fundus images) and a testing set (20 Fundus images). This public

CHASE_DB1 database consists of 28 retinal fundus images from 14 patients' left and right eyes, each with a 30-degree field of vision. This database contains photos with a resolution of 999×960 pixels that were taken with a Nidek NM200D camera but suffer from poor contrast and lighting issues.

2.1.3. DRIONS-DB

The DRIONS dataset [33] was created using images from patients (men 46.2% and women 53.8%) of Caucasian ethnicity at the Ophthalmology Service at Miguel Servet Hospital in Saragossa, Spain. Two independent experts painstakingly separated the OD. There are 110 color images with a resolution of 600×400 in the collection.

2.2. Pre-processing

Fundus images must be preprocessed using normalization and low light enhancement [34] in order to achieve improved accuracy for segmentation and feature extraction for learning models. The developed preprocessing is used to overcome the issues of misalignments of retinal and camera focus, lightning conditions, and errors in the camera that affect fundus images. The normalization method is more effective at removing impulse and machinery noises and also helps to increase image quality significantly. In this research study, the conversion of color images into grayscale images is achieved. Normalization of grayscale images is performed according to (1).

$$I_N = (I - Min) \times \frac{newMax - newMin}{Max - Min} + newMin \tag{1}$$

An n-dimensional grayscale picture I with intensity values between (Min, Max) is transformed via normalization into a new image I_N with intensity values between $(newMin, newMax)$.

To reduce all types of aberrations in the frequency levels, the convolution property is used to improve the fundus image. This manages the fundus image's dark level and changes the contrast for better pixel density distribution within the specified range, resulting in enhanced images. In the test, all techniques for segmenting the OD employ the beginning contours shown in section 2.3 for computing the evolution contour. In the vessel-free image, all contrastive segmentation techniques are computed. The proposed objective functions are optimized to get the final segmentation results for the OD.

2.3. Optic disk localization

The entropy-based localization is performed to locate the exact position according to the contrast of the optical disc. Here, the portion with higher contrast has huge entropy which is used to locate the OD precisely in the overall image. The optical disc area has more precise data that can be utilized to recognize it. Hence, OD's identification in the landmark fundal is significant to monitor the changes in the OD.

Information measurement is associated with an information theory, and it has been crucial in a variety of application areas, including image analysis. It is possible to interpret the entropy of a probability distribution as both a measure of information as well as a measure of uncertainty. Formally, let X is the discrete random variable and the probability mass function is $(x), x \in X$. The Shannon entropy for the discrete random variable X is described as (2),

$$H(X) = \sum_{x \in X} p(x) \log p(x) \tag{2}$$

where $p(x) \in [0.0, 1.0], (-\log p(x))$ is an information association for occurrence x, and $\sum_{x \in X} p(x) = 1$.

In a digital image, the pixel values of the variation are transmitting the information inside the image that is being evaluated by the entropy metric. However, the image features a range of scattered brightness values; image entropy H_I can be calculated as (3),

$$H_I = -\sum_{j=0}^{M_g - 1} p(j) \log_2 p(j) \tag{3}$$

where $p(j)$ is the brightness value of distribution indexed by j inside image I; M_g is total of brightness stages in an interested image I. In the processing stages of images, measuring the entropy creates a value that develops the novel characteristics that are exploited in image investigation like texture analysis. Entropy of the low values is recommended for the texture of smoothing, as texture with more information entails entropy of higher values. Hence, its capabilities are utilized to create a novel feature to determine the texture smoothing of images. There is additional information, such as nerves and blood vessels going through, in the region of the OD in the fundus image. That means it is not smooth in texture. It is expected that its entropy value can be higher than the fundus images of regions.

This technique has been used to locate objects in images. Regardless of how the image is broken into sub images (regions), each one will be evaluated independently using the quality function. As a result, the location with the highest score will be considered for the region of interest. Assume X is a region-partitioned image, divided into subregions (4).

$$X = \{R_1, R_{2,........}, R_n\} \tag{4}$$

However, R_i represents the region labeled with (top, bottom, left, and right) coordinates, $f(R_i)$ represents an excellence function or a quality function, and x_j represents the candidate region with $R_{j=argmax_{R_i \in x} f(R_i)}$.

In this study, a sliding window technique with two distinct methods nonoverlap and overlap is considered as the proposed methodology. However, each image pixel in the nonoverlap approach cannot be a part of more than one region, so it becomes (5).

$$R_i \cap R_j = 0 \tag{5}$$

Meanwhile, the overlap approach permits an image to be a part of many regions.

$$R_i \cap R_j \neq 0/ \tag{6}$$

R_i, R_j are regions in the image.

2.4. Optic disc segmentation

In SL-EACM, the saliency map is initially generated according to the image shape, color, and textures. Information from the generated saliency map is given as input to level set for detecting the boundary of OD. Therefore, an edge indicator of level set with enhanced active contour effectively predicts the OD's boundary by using the saliency map information. Other factors, such as blood vessel coverage, image variations, and border smoothing near the OD's boundary induced by pathological alterations, complicate the OD segmentation. In order to solve the aforementioned issues, multi-view data is extracted based on the appearance and shape of OD with the goal of achieving accurate OD detection under a variety of scenarios. The SL-EACM is augmented by including the local image probability information from a multi-dimensional feature space surrounding the site of interest (SLACM-A), which is based on the appearance of OD. In a single feature space, for the jth object at pixel x, the Gaussian probability density function (PDF) is described based on the transformed domain.

$$P\left(I'\left(\frac{x}{\theta_j}, B\right)\right) \propto \prod_{y \in \Omega_j \cap O_x} P(I(y|\theta_j, B, x)) \tag{7}$$

where

$$P\left(I(y|\theta_j, B, x)\right) = \frac{1}{\sqrt{2\pi}\sigma_j} \exp(-\frac{\left(I(y) - B(x)c_j\right)^2}{2\sigma_j^2})$$

where, in the transformed domain, the image is represented by I'. In a single feature space, for the jth object at the pixel y near the pixel x the Gaussian PDF is given by $P(I(y|\theta_j, B, x))$. Π is indicated as multiplication. θ_j indicates the group of estimated parameters $\{cj, \sigma j\}$. Now the functioning mechanism is combined with probability data from multidimensional feature space. At the pixel x for the jth object based on the transformed domain; the proposed probability function based on the mentioned Gaussian PDF for the transformed domain is depicted in (8). It integrates a more detailed version of the local image probability data collected at the point of interest over a multi-dimensional feature space.

$$\prod_{i=1}^{d} P_i(I_i'(x/\theta_{ji}, B_i)) \propto \prod_{i=1}^{d} \prod_{y \in \Omega_j \cap O_x} P\left(I(y|\theta_j, B, x)\right) \tag{8}$$

where

$$P_i(I_i(y|\theta_{ji}, B_i, x))) = \frac{1}{\sqrt{2\pi}\sigma_{ji}} \exp(-\frac{\left(I_i(y) - B_i(x)c_{ji}\right)^2}{2\sigma_{ji}^2}))$$

where the total of feature spaces is indicated by d. θ_{ji} indicates the group of estimated parameters $\{c_{ji}, \sigma_{ji}\}$. In the ith feature space, the input image is referred to as I_i. For the ith feature space, the image in the transformed domain is referred to as I_i'. In the ith feature space, at pixel x for the jth object the Gaussian PDF based on the transformed domain is $P_i(I_i'\left(\frac{x}{\theta_{ji}}, B_i\right))$.

In the ith feature space, at the local region $\Omega_j \cap O_x$ centered at each location x, the spatial varying mean that is estimated is denoted by $B_i(x)c_{ji}$. In i^{th} feature space, the bias field function is denoted by B_i. In the ith feature space the true signal of the jth object is assumed to be c_{ji}. In the ith feature space, for the jth object, the standard deviation of the Gaussian distribution is denoted by σ_{ji}. Assuming that

$$D = \{I'(x/\theta_{ji}, B_i), x \in \Omega, j = 1, \dots, n; i = 1, \dots, d\},$$

the proposed probability function, which combines probability data with multidimensional attributes, can be used to represent the joint likelihood function as (9),

$$P(\tfrac{D}{\theta}, B) = \prod_{j=1}^n \prod_{x \in \Omega} \prod_{i=1}^d P_i\left(I_i'\left(x / \theta_{ji}, B_i\right)\right) \propto \prod_{j=1}^n \prod_{x \in \Omega} \prod_{i=1}^d P_i(I_i'(y/\theta_{ji}, B_i, x) \tag{9}$$

where $\theta = \{\theta_{ji}, j = 1, \dots, n; i = 1, \dots, d\}, B = \{B_i, i = 1, \dots, d\}, n$ describes the total of objects. The inverse log-likelihood function of $P(\tfrac{D}{\theta}, B)$ is defined in order to evaluate the parameter set $\theta^\sim$ and $B^\sim$. In the meantime, the constant weight coefficient is added and the trivial constant term is eliminated.

To obtain the new method based on appearance, use (10),

$$E_{SLEACM-A} = \frac{1}{d} \sum_{i=1}^d \sum_{j=1}^n \int_\Omega F_{ji}(y) M_j(\phi(y)) dy \tag{10}$$

where

$$F_{ji}(y) \triangleq \int_\Omega K_\rho(x, y)(\log(\sigma_{ji}) + ((I_i(y) - B_i(x)c_{ji})^2 / 2\sigma_{ji}^2)) dx$$
$$M_1 = H(\phi(y)); \quad M_2 = 1 - H(\phi(y))$$

In the retinal color fundus images, because the area of optic disc (OD) is brighter in comparison with other areas, the number of objects n is taken as 2; $c_{1i} = (c_{11}, c_{12}, \dots, c_{1d}), c_{2i} = (c_{21}, c_{22}, \dots, c_{2d}), B_1 = (B_1, B_2, \dots, B_d), \sigma_{1i} = (\sigma_{11}, \sigma_{12}, \dots, \sigma_{1d})$ and $\sigma_{1i} = (\sigma_{21}, \sigma_{22}, \dots, \sigma_{2d})$ are five steady vectors. In i^{th} feature space, the true signal of the OD and the background is assumed to be the values of the two vectors namely c_{1i} and c_{2i}, respectively. H indicates the Heaviside function. In the ith feature space, the values of the two vectors σ_{1i} and σ_{2i} respectively, represents the standard deviation of the Gaussian distribution of the OD and the background. For segmenting the OD, the level set function is represented by ϕ. The energy function in (5) is minimized, so the values of $c_{1i}, c_{2i}, B_i \sigma_{1i}$ and σ_{2i} are optimally chosen.

Because of the complicated OD appearance (e.g., illumination changes, anomalous effects, and interlaced blood arteries), a single feature space cannot adequately describe the entire OD. As a result, the multi-feature spaces must be merged in order to complement each other's advantages for effectively representing the OD. The red color plane offers a subtle contrast for blood vessels and provides better contrast for the OD region, and the hue-saturation-value (HSV) color space can easily separate the intensity information from the color information and extract additional information. The expanded SL-EACM then uses a multi-dimensional feature space ($d = 5$) to describe an image point x, with each vector element drawn from the red color plane, vessel-free red color plane, and each channel from vessel-free HSV color space.

Given that the OD has a circular or elliptical shape, the SL-EACM incorporates OD shape priori information while keeping the fundamental anatomical structure. Initially, the OD's elliptic parameterized level set function which consists of a five-tuple ($x_d, y_d, \theta_d, a_d, b_d$) is introduced. It can be described as (11),

$$\phi_0 = 1 - \sqrt{\left(\frac{A^2}{a_d^2}\right) + \left(\frac{B^2}{b_d^2}\right)} \tag{11}$$

where

$$A = (x - x_d)dx \cos\theta_d + (y - y_d)s\,\theta_d$$
$$B = -(x - x_d)\sin\theta_d + (y - y_d)\cos\theta_d$$

where the scaling factor of the semi-major axis length is defined as a_d and the semi-minor axis length is denoted by b_d. Furthermore, x_d and y_d are oval center coordinates, and the angle of rotation is θ_d. Then, using the elliptic parameterized level set function ϕ_0 for the OD, an ellipse constraint term is created. It can be shown as (12),

$$E_{ShapePrior} = \int_\Omega v \left(H(\phi(y)) - H(\phi_0(y)) \right)^2 dy \tag{12}$$

where

$$\phi_0 = 1 - \sqrt{\left(\frac{A^2}{a_d^2}\right) + \left(\frac{B^2}{b_d^2}\right)}$$

where $A = (x - x_d)dx \cos\theta_d + (y - y_d)\sin\theta_d$, $B = -(x - x_d)\sin\theta_d + (y - y_d)\cos\theta_d$ and the weight of elliptic constraint is determined using the constraint coefficients for ellipse v. The expression (12) simultaneously drives φ and φo, and it is symmetric to φ and φo to constrain the zero-level set of φ as an ellipse. It is possible to write the extended SL-EACM by integrating the ellipse constraint term (13),

$$E = \sum_{j=1}^{n} \int_\Omega F_j(y)M_j(\phi(y))dy + \int_\Omega v \left(H(\phi(y)) - H(\phi_o(y)) \right)^2 dy \tag{13}$$

where

$$F_j(y) \triangleq \int_\Omega K_\rho(x,y)(\log(\sigma_j) + ((t(y) - B(x)c_j)^2 / 2\sigma_j^2)), M_1 = H(\phi(y)), M_2 = 1 - H(\phi(y))$$

where, as in the previous section, the number of objects n is also set as 2.

Both of them constantly change with the curve evolution. Furthermore, the penalized length item is utilized to regularize the level set function (LSF) φ zero level contour in order to extract a smoother contour with less error and concavity. In addition, with (14) the entire energy function can be described as:

$$E_{LSACM-S} = \sum_{j=1}^{n} \int_\Omega F_j(y)M_j dy + \int_\Omega \lambda \left| \nabla H(\phi_o(y)) \right|^2 dy + \int_\Omega v \left(H(\phi_o(y)) \right)^2 dy \tag{14}$$

where λ is referred to as the length-weight of the zero-stage curve of ϕ.

As a result, the initialization of level set function LSF can be done in a variety of ways. Using a checkerboard form, the level set function is initialized as opposed to the traditional method of drawing a box inside or outside the object. Checkerboard is described as:

$$\phi(x,y) = c \times \sin\left(\frac{\pi \times R \times x}{1500}\right) \times \sin\left(\frac{\pi \times C \times y}{1500}\right) \tag{15}$$

where C represents the input image's width, and R represents the input image's height, c defines the amplitude of the initial LSF representing a positive number, and $0 < c < 1$ is set in the application.

3. RESULTS AND DISCUSSION

The detected area is initially evaluated based on the area overlap between the generated segmentation region and expert-marked ground truth. In order to evaluate the detected area, the following pixel-wise precision and recall values must be calculated and defined as (16) and (17),

$$Precision = \frac{TP}{TP+FP} \tag{16}$$

$$Recall = \frac{TP}{TP+FN} \tag{17}$$

where TN is referred to as the worth of the true negative, TP is referred to as the worth of the true positive, FP denotes the worth of the false positive, and FN denotes the worth of the false negative. The OD segmentation results are obtained using a calculation based on i) the original retinal color fundus images, ii) the ground truth-based OD segmentation result, and iii) the result of the proposed method's OD segmentation. Then, a metric that represents the harmonic mean of precision and recall, known as the standard F-score, is calculated using (18).

$$F - \text{score (F)} = 2 * \frac{(Precision)(Recall)}{Precision + Recall} \tag{18}$$

The F-score value is always between 0 and 1. A high F-score may be a sign of effective segmentation performance. Second, the distance between the boundary obtained by the algorithm and the actual situation is used to evaluate the border. The results of CHASE_DB, DRIONS-DB, and Drishti-GS database images have been shown in Table 1, as well as the suggested method's output pictures with regard to input images from the CHASE_DB, DRIONS-DB, and Drishti-GS databases, respectively. The table is displayed, starting with the row of input images, one from each dataset that underwent preprocessing. The preprocessed image's calculated entropy value is displayed in the next row. A cropped disc is given for the original set of photographs after the disc localization procedure has been completed. In the last two rows, you can see the produced segmented disc picture and the ground truth.

Table 1. Segmented images using different datasets

Dataset	CHASE_DB	DRIONS-DB	Drishti-GS
Input Image			
Preprocessed Image			
Entropy calculation			
Disk Localization			
Cropped Disk in Original Image			
Ground truth			
Segmented Disk Image			

The comparison between the level set, the saliency-based level set with an enhanced active contour method (SL-ACM) [35], and the SL-EACM is shown in Table 2. From the analysis, it is known that the SL-EACM provided better accuracy than the level set and SL-ACM for all the datasets of CHASE_DB, DRIONS-DB, and Dristhi-DS. The enhanced active contour along with the saliency map used in the SL-EACM has information on color, shape, and textures which helps to enhance OD segmentation. More specifically, the enhanced contour function used in the level set of SL-EACM is used to overcome the issues of illumination.

Table 3 shows the comparison of the SL-ACM and SL-EACM with and without preprocessing methods. The table proves that both SL-ACM and SL-EACM have better performances when operated with the preprocessing method. The normalization and low light enhancement-based preprocessing is used to overcome the issues of misalignments of retinal and camera focus, lightning condition, and errors in the camera that affects fundus images. Further, the SL-EACM outperforms well when compared to the SL-ACM. The edge indicator along with saliency map information used in the SL-EACM enhances the performances of OD segmentation.

Table 2. Comparison of various methods

Dataset	Methods	Jaccard	Dice	Accuracy	Sensitivity
CHASE_DB	Level set	0.2989	0.8242667	0.9334	0.788
	SL-ACM (Existing)	0.0791	0.9588204	0.98897879	1
	SL-EACM (Proposed)	0.039517	0.9798433	0.99445950	1
DRIONS-DB	Level set	0.15756220	0.9144816	0.8865	0.8424
	SL-ACM (Existing)	0.07331628	0.9619469	0.98457429	1
	SL-EACM (Proposed)	0.03358908	0.9829185	0.99214764	0.96641091
Drishti-DS	Level set	0.33545715	0.798468	0.7573	0.9443
	SL-ACM (Existing)	0.06087685	0.9686059	0.99131058	0.94559257
	SL-EACM (Proposed)	0.05810867	0.9700762	0.99170918	0.94798256

Table 3. Effect of pre-processing techniques for existing and proposed model

Dataset	Methods		Jaccard	Dice	Accuracy	Sensitivity	Precision	F-Measure
CHASE_DB	SL-ACM	Without Pre-processing	0.0842	0.9415	0.9759	1	0.925766	0.961452
		With Pre-processing	0.0791	0.9588	0.989	1	0.920898	0.95882
	SL-EACM	Without Pre-processing	0.1079	0.943	0.9849	0.8704	0.892111	0.881122
		With Pre-processing	0.0395	0.9798	0.9945	1	0.960483	0.979843
DRIONS-DB	SL-ACM	Without Pre-processing	0.0816	0.9575	0.9862	1	0.918398	0.957464
		With Pre-processing	0.0733	0.9619	0.9846	1	0.926684	0.961947
	SL-EACM	Without Pre-processing	0.0906	0.9525	0.9781	0.9094	1	0.952551
		With Pre-processing	0.0336	0.9829	0.9921	0.9664	1	0.982913
Drishti-GS1	SL-ACM	Without Pre-processing	0.0837	0.9563	0.9889	0.9169	0.999345	0.956349
		With Pre-processing	0.0609	0.9686	0.9913	0.9456	0.992768	0.96861
	SL-EACM	Without Pre-processing	0.0888	0.9535	0.9837	0.9129	0.997353	0.95326
		With Pre-processing	0.0581	0.9701	0.9917	0.948	0.993224	0.970085

4.   CONCLUSION

Since glaucomatous damage cannot be reversed, automated glaucoma evaluation is important for both early identification and therapy. This research presents a unique model for segmenting the OD for glaucoma diagnosis. A brand-new segmentation model is proposed for accurately retrieving the OD border. To address the often-recurring intensity inhomogeneity problem, SL-EACM is first introduced. The preprocessing method is used to alter SL-EACM in order to steer the evolution of the OD contour in a useful region and reduce the detrimental influence of non-objects. It can go beyond the standard active contour method (ACM)'s inability to directly segment the OD. The SL-EACM model is improved by including the local image probability data from the multi-dimensional feature space surrounding the point of interest in order to overcome the lack of data for the single-feature space. The shape priori constraint information is incorporated into the model, which helps to further strengthen the robustness of the changes found in and around object areas since the segmentation objects share an elliptical shape structure. The results of the experiments on the above-mentioned datasets demonstrated that the suggested strategy outperforms other cutting-edge methods such as level set and SL-ACM. The accuracy of the SL-EACM is 0.9917 for the Drishti-DS dataset which is higher than the level set and SL-ACM. Even while the recommended method can successfully segment most typical fundus pictures with reduced OD diameters, occasionally it might not work. Moving the priors to the location of the OD will help us avoid this issue in the future.

REFERENCES

[1]   A. Chakravarty and J. Sivaswamy, "Joint optic disc and cup boundary extraction from monocular fundus images," *Computer Methods and Programs in Biomedicine*, vol. 147, pp. 51–61, Aug. 2017, doi: 10.1016/j.cmpb.2017.06.004.

[2]   J. Cheng, F. Yin, D. W. K. Wong, D. Tao, and J. Liu, "Sparse dissimilarity-constrained coding for glaucoma screening," *IEEE Transactions on Biomedical Engineering*, vol. 62, no. 5, pp. 1395–1403, May 2015, doi: 10.1109/TBME.2015.2389234.

[3]   J. Zilly, J. M. Buhmann, and D. Mahapatra, "Glaucoma detection using entropy sampling and ensemble learning for automatic optic cup and disc segmentation," *Computerized Medical Imaging and Graphics*, vol. 55, pp. 28–41, Jan. 2017, doi: 10.1016/j.compmedimag.2016.07.012.

[4]   M. S. Haleem *et al.*, "A novel adaptive deformable model for automated optic disc and cup segmentation to aid glaucoma diagnosis," *Journal of Medical Systems*, vol. 42, no. 1, Jan. 2018, doi: 10.1007/s10916-017-0859-4.

[5]   J. Zong, T. Qiu, W. Li, and D. Guo, "Automatic ultrasound image segmentation based on local entropy and active contour model," *Computers and Mathematics with Applications*, vol. 78, no. 3, pp. 929–943, Aug. 2019, doi: 10.1016/j.camwa.2019.03.022.

[6]   N. Harizman, "The ISNT rule and differentiation of normal from glaucomatous eyes," *Archives of Ophthalmology*, vol. 124, no. 11, Nov. 2006, doi: 10.1001/archopht.124.11.1579.

[7]   S. Sekhar, W. Al-Nuaimy, and A. K. Nandi, "Automated localisation of retinal optic disk using Hough transform," in *2008 5th IEEE International Symposium on Biomedical Imaging: From Nano to Macro*, May 2008, pp. 1577–1580, doi: 10.1109/ISBI.2008.4541312.

[8]   A. Bhuiyan, R. Kawasaki, T. Y. Wong, and R. Kotagiri, "A new and efficient method for automatic optic disc detection using geometrical features," in *IFMBE Proceedings*, Springer Berlin Heidelberg, 2009, pp. 1131–1134.

[9]   X. Bian, X. Luo, C. Wang, W. Liu, and X. Lin, "Optic disc and optic cup segmentation based on anatomy guided cascade network," *Computer Methods and Programs in Biomedicine*, vol. 197, Dec. 2020, doi: 10.1016/j.cmpb.2020.105717.

[10] H. Li and O. Chutatape, "Boundary detection of optic disk by a modified ASM method," *Pattern Recognition*, vol. 36, no. 9, pp. 2093–2104, Sep. 2003, doi: 10.1016/S0031-3203(03)00052-9.

[11] J. Cheng *et al.*, "Superpixel classification based optic disc and optic cup segmentation for glaucoma screening," *IEEE Transactions on Medical Imaging*, vol. 32, no. 6, pp. 1019–1032, Jun. 2013, doi: 10.1109/TMI.2013.2247770.

[12] N. Thakur and M. Juneja, "Survey on segmentation and classification approaches of optic cup and optic disc for diagnosis of glaucoma," *Biomedical Signal Processing and Control*, vol. 42, pp. 162–189, Apr. 2018, doi: 10.1016/j.bspc.2018.01.014.

[13] Xiaolu Zhu and R. M. Rangayyan, "Detection of the optic disc in images of the retina using the Hough transform," in *2008 30th Annual International Conference of the IEEE Engineering in Medicine and Biology Society*, Aug. 2008, pp. 3546–3549, doi: 10.1109/IEMBS.2008.4649971.

[14] A. Aquino, M. E. Gegúndez-Arias, and D. Marín, "Detecting the optic disc boundary in digital fundus images using morphological, edge detection, and feature extraction techniques," *IEEE Transactions on Medical Imaging*, vol. 29, no. 11, pp. 1860–1869, Nov. 2010, doi: 10.1109/TMI.2010.2053042.

[15] M. Lalonde, M. Beaulieu, and L. Gagnon, "Fast and robust optic disc detection using pyramidal decomposition and Hausdorff-based template matching," *IEEE Transactions on Medical Imaging*, vol. 20, no. 11, pp. 1193–1200, 2001, doi: 10.1109/42.963823.

[16] J. Cheng *et al.*, "Automatic optic disc segmentation with peripapillary atrophy elimination," in *2011 Annual International Conference of the IEEE Engineering in Medicine and Biology Society*, Aug. 2011, pp. 6224–6227, doi: 10.1109/IEMBS.2011.6091537.

[17] Y. Gao, X. Yu, C. Wu, W. Zhou, X. Lei, and Y. Zhuang, "Automatic optic disc segmentation based on modified local image fitting model with shape prior information," *Journal of Healthcare Engineering*, pp. 1–10, Mar. 2019, doi: 10.1155/2019/2745183.

[18] A. Septiarini, A. Harjoko, R. Pulungan, and R. Ekantini, "Optic disc and cup segmentation by automatic thresholding with morphological operation for glaucoma evaluation," *Signal, Image and Video Processing*, vol. 11, no. 5, pp. 945–952, Jul. 2017, doi: 10.1007/s11760-016-1043-x.

[19] A. Osareh, M. Mirmehdi, B. T. Thomas, and R. Markham, "Colour morphology and snakes for optic disc localisation," In *The 6th medical image understanding and analysis conference*, 2002.

[20] G. D. Joshi, J. Sivaswamy, and S. R. Krishnadas, "Optic disk and cup segmentation from monocular color retinal images for glaucoma assessment," *IEEE Transactions on Medical Imaging*, vol. 30, no. 6, pp. 1192–1205, Jun. 2011, doi: 10.1109/TMI.2011.2106509.

[21] P. S. Mittapalli and G. B. Kande, "Segmentation of optic disk and optic cup from digital fundus images for the assessment of glaucoma," *Biomedical Signal Processing and Control*, vol. 24, pp. 34–46, Feb. 2016, doi: 10.1016/j.bspc.2015.09.003.

[22] Fengshou Yin *et al.*, "Model-based optic nerve head segmentation on retinal fundus images," in *2011 Annual International Conference of the IEEE Engineering in Medicine and Biology Society*, Aug. 2011, pp. 2626–2629, doi: 10.1109/IEMBS.2011.6090724.

[23] T. Chan and L. Vese, "An active contour model without edges," in *International Conference on Scale-Space Theories in Computer Vision*, 2002, pp. 141–151.

[24] J. Lowell *et al.*, "Optic nerve head segmentation," *IEEE Transactions on Medical Imaging*, vol. 23, no. 2, pp. 256–264, Feb. 2004, doi: 10.1109/TMI.2003.823261.

[25] J. Xu, O. Chutatape, E. Sung, C. Zheng, and P. Chew Tec Kuan, "Optic disk feature extraction via modified deformable model technique for glaucoma analysis," *Pattern Recognition*, vol. 40, no. 7, pp. 2063–2076, Jul. 2007, doi: 10.1016/j.patcog.2006.10.015.

[26] A. Sevastopolsky, "Optic disc and cup segmentation methods for glaucoma detection with modification of U-Net convolutional neural network," *Pattern Recognition and Image Analysis*, vol. 27, no. 3, pp. 618–624, Jul. 2017, doi: 10.1134/S1054661817030269.

[27] H. Fu, J. Cheng, Y. Xu, D. W. K. Wong, J. Liu, and X. Cao, "Joint optic disc and cup segmentation based on multi-label deep network and polar transformation," *IEEE Transactions on Medical Imaging*, vol. 37, no. 7, pp. 1597–1605, Jul. 2018, doi: 10.1109/TMI.2018.2791488.

[28] S. Yu, D. Xiao, S. Frost, and Y. Kanagasingam, "Robust optic disc and cup segmentation with deep learning for glaucoma detection," *Computerized Medical Imaging and Graphics*, vol. 74, pp. 61–71, Jun. 2019, doi: 10.1016/j.compmedimag.2019.02.005.

[29] Y. Yi, J. Wang, W. Zhou, C. Zheng, J. Kong, and S. Qiao, "Non-negative matrix factorization with locality constrained adaptive graph," *IEEE Transactions on Circuits and Systems for Video Technology*, vol. 30, no. 2, pp. 427–441, Feb. 2020, doi: 10.1109/TCSVT.2019.2892971.

[30] Y. Yi, J. Wang, W. Zhou, Y. Fang, J. Kong, and Y. Lu, "Joint graph optimization and projection learning for dimensionality reduction," *Pattern Recognition*, vol. 92, pp. 258–273, Aug. 2019, doi: 10.1016/j.patcog.2019.03.024.

[31] J. Sivaswamy, S. R. Krishnadas, A. Chakravarty, G. D. Joshi, Ujjwal, and T. A. Syed, "A comprehensive retinal image dataset for the assessment of glaucoma from the optic nerve head analysis," *JSM Biomedical Imaging Data Papers*, vol. 2, no. 1, pp. 1–7, 2015.

[32] W. Zhou, S. Qiao, Y. Yi, N. Han, Y. Chen, and G. Lei, "Automatic optic disc detection using low-rank representation based semi-supervised extreme learning machine," *International Journal of Machine Learning and Cybernetics*, vol. 11, no. 1, pp. 55–69, Jan. 2020, doi: 10.1007/s13042-019-00939-0.

[33] M. S. Haleem, L. Han, J. van Hemert, and B. Li, "Automatic extraction of retinal features from colour retinal images for glaucoma diagnosis: A review," *Computerized Medical Imaging and Graphics*, vol. 37, no. 7–8, pp. 581–596, Oct. 2013, doi: 10.1016/j.compmedimag.2013.09.005.

[34] S. Naz, R. K. R. K. A, and S. T, "EFPT-OIDS: evaluation framework for a pre-processing techniques of automatic optho-imaging diagnosis and detection system," *International Journal of Advanced Computer Science and Applications*, vol. 12, no. 11, 2021, doi: 10.14569/IJACSA.2021.0121151.

[35] X.-H. Zhi and H.-B. Shen, "Saliency driven region-edge-based top down level set evolution reveals the asynchronous focus in image segmentation," *Pattern Recognition*, vol. 80, pp. 241–255, Aug. 2018, doi: 10.1016/j.patcog.2018.03.010.

BIOGRAPHIES OF AUTHORS

Sobia Naz 🔗 completed her B.E. from P.E.S. College of Engineering, in 2008 and M. Tech from Sri Jayachamarajendra College of Engineering, VTU, Belgaum in 2014. She is currently pursuing her Ph.D. She has more than 12 years of teaching experience and her areas of interest are medical image processing, bio-medical signal processing, and machine learning. She can be contacted at sobia.pesce@gmail.com.

Kabbinale Ananda Radhakrishna Rao 🔗 graduated from University of Mysore, Karnataka in Electronics and Communication Engineering in 1984. He obtained his master's degree and Ph.D. from IIT, Madras and IISc, Bangalore in 1989 and 2004, respectively. He is serving P.E.S. College of Engineering, Mandya since 1985 at various levels. He has a vast teaching experience of more than 35 years and has guided several UG and PG projects. He has guided several research students in his career. He has several publications to his contributions. During his career, he has taken up several funded projects. His areas of interest are signal processing, image processing, DSP, DSP processor, microprocessor and controller, and advanced embedded system design. He can be contacted at karkrao@gmail.com.